PRAMANA
— journal of
physics

Vol. 78, No. 4
April 2012
pp. 565–584

Design of a superconducting low beta niobium resonator

PRAKASH N POTUKUCHI* and AMIT ROY

Inter-University Accelerator Centre, Aruna Asaf Ali Marg, New Delhi 110 067, India
*Corresponding author. E-mail: prakash@iuac.res.in

MS received 12 June 2011; accepted 8 December 2011

Abstract. The proposed high current injector for the superconducting Linac at the Inter-University Accelerator Centre will have several accelerating structures, including a superconducting module which will contain low beta niobium resonators. A prototype resonator for the low beta module has been designed. The resonator has been carefully modelled to optimize the electromagnetic parameters. In order to validate them, a room-temperature copper model has been built and tested. In this paper we present details of the electromagnetic design of the low beta resonator, briefly discuss the mechanical and engineering design, and present results from the measurements on the room-temperature copper model.

Keywords. Superconducting niobium resonator; linear accelerator.

PACS Nos 29.20.Ej; 85.25.–j; 29.27.–a

1. Introduction

The 15 UD Pelletron accelerator at the Inter-University Accelerator Centre (IUAC) [1] currently injects heavy ion beams into the superconducting booster Linac [2]. The Pelletron accelerator cannot deliver large beam currents at higher charge states due to design and operational constraints. In the last few decades much progress has been made in extracting hundreds of μA of beam current at high charge states from electron cyclotron resonance (ECR) ion sources [3]. The proposed high current injector (HCI) at IUAC [4] plans to exploit this to provide an alternate injector for the superconducting Linac. In figure 1, a block diagram of the HCI system is shown. The low energy ion beam of mass to charge ratio $(A/q) = 6$ from the high-temperature superconducting ECR (HTS-ECR) ion source at an energy of about 7.5 keV/u would be injected into a room temperature radiofrequency quadrupole (RFQ). The RFQ would further accelerate the beam to about 180 keV/u for injection into the drift tube Linac (DTL). The DTL section would consist of half a dozen tanks, which would accelerate the beam to about 1.5 MeV/u.

The main superconducting Linac consists of three cryomodules each containing eight niobium quarter-wave resonators [5]. In figure 2, a schematic diagram of the two-gap accelerating system such as the quarter-wave resonator, is shown. For a particle to gain

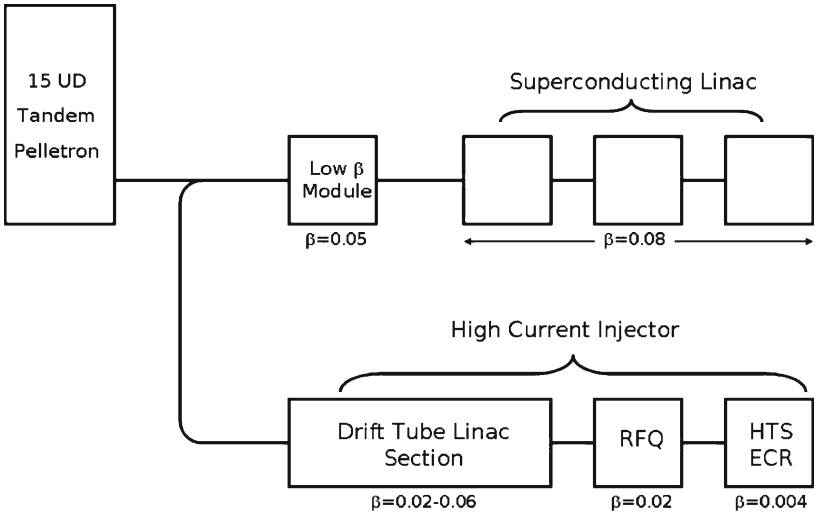

Figure 1. Block diagram of the proposed high current injector (HCI) system at IUAC.

maximum energy while passing through it, the particle velocity β ($=v/c$; c being the velocity of light) should be such that the phase of the applied RF (radiofrequency) changes by π radians during the time the particle takes to travel from the centre of the first gap to the centre of second gap (d), i.e.,

$$d = \frac{\beta\lambda}{2},$$

where λ is the wavelength of the RF. This condition is exactly satisfied for a unique velocity β_0, referred to as the synchronous velocity. For other velocities, the energy gain is given in terms of the transit time factor $T(\beta)$, as

$$E_{\text{Gain}} = qE_{\text{a}}L_{\text{eff}}T(\beta)\,,$$

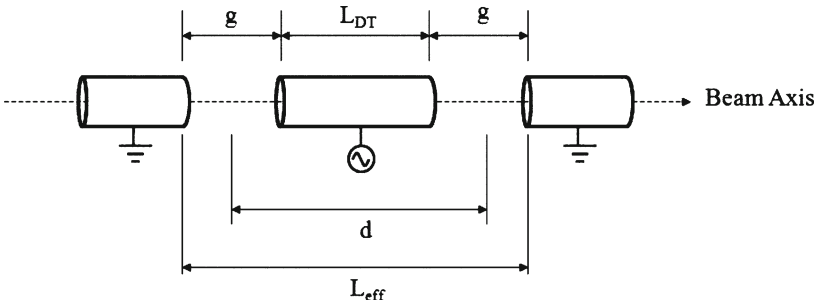

Figure 2. Schematic diagram of a two-gap accelerating system. The drift tube of length L_{DT} is in the middle. The two tubes at either end of the drift tube are the ports on the outer housing. The acceleration takes place in the two gaps (each of length g).

where q is the charge state of the ion, E_a is the average accelerating electric gradient which is averaged over the effective acceleration length L_{eff} and $T(\beta)$ is the ratio of the energy gained by a particle of any velocity to that gained by the particle of synchronous velocity, that is,

$$T(\beta)=\frac{\int_{-L_{\text{eff}}/2}^{+L_{\text{eff}}/2} E(z)\sin(\omega t+\phi)\,\mathrm{d}z}{\max\int_{-L_{\text{eff}}/2}^{+L_{\text{eff}}/2} E(z)\sin(\omega t+\phi)\,\mathrm{d}z},$$

where $E(z)\sin(\omega t+\phi)$ is the longitudinal electric field experienced by the particle along the beam axis and $\omega = 2\pi f$ is the angular frequency of the applied RF. Obviously $T(\beta_0) = 1$.

The resonators in the superconducting Linac operate at 97 MHz and are optimized for the synchronous velocity $\beta_0 = 0.081$. In figure 3, $T(\beta)$ as a function of β, for this resonator, is shown. The range of velocities which can be accelerated by the resonator with a minimum efficiency of at least, say 70%, is given by $\Delta\beta = \beta_{\text{high}} - \beta_{\text{low}}$, where β_{low} and β_{high} are the lower and upper cut-offs at 70% of the maximum energy gain (see figure 3). As can be seen, the value of $T(\beta)$ at $\beta = 0.054$ is around 0.7, which rapidly falls to less than 0.5 at $\beta = 0.049$, which is quite low.

The beam energy out of the DTL section is about 1.5 MeV/u, which corresponds to $\beta \approx 0.057$. This is very close to the lower velocity cut-off β_{low} of the quarter-wave resonators employed in the superconducting Linac. In order to provide some extra cushion for velocity matching of the beam out of the DTL section into the main Linac, a superconducting module containing low beta resonators has been planned. The low beta module would be so placed that it can accelerate beams from HCI as well as from the Pelletron accelerator for injection into the superconducting Linac (see figure 1). This would also

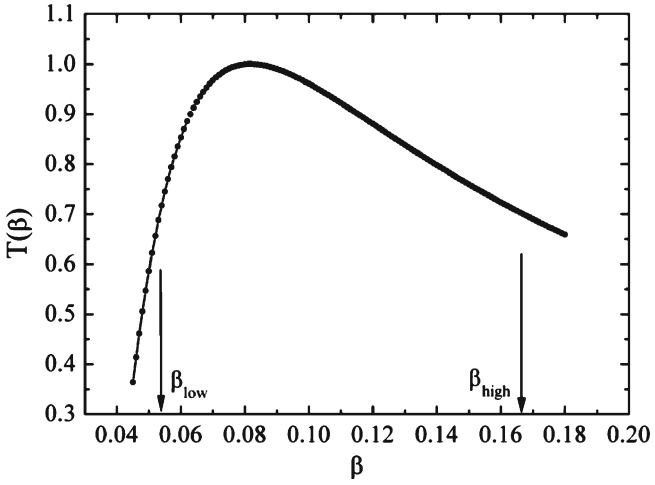

Figure 3. Transit time factor $T(\beta)$ vs. β for the quarter-wave resonators installed in the superconducting Linac. The two velocities β_{high} and β_{low} indicate the range for which the energy gain is more than 70% of the maximum.

allow acceleration of heavier beams (mass > 130) from the Pelletron accelerator through the superconducting Linac than what is currently possible.

2. Low β resonator design

TEM class superconducting niobium resonators have been used in Linacs for accelerating heavy ion beams [6]. They are usually designed in the frequency range 50–150 MHz where the Bardeen–Cooper–Schrieffer (BCS) surface resistance of superconducting niobium is small enough to permit their operation at 4.2 K. Several variants of this class of structures have been designed and developed [7]. Of these, the two-gap quarter-wave resonator (QWR) is characterized by its excellent mechanical stability and broad velocity acceptance. In general, QWRs have performed better than other structures in its class [8]. In addition, they are easier to fabricate compared to other designs, although more number of resonators are needed for achieving the required energy gain. For these reasons the two-gap co-axial line quarter-wave resonator has been chosen for the low beta resonator design.

2.1 *Key parameters for optimization*

Superconducting niobium resonators are always designed to maximize the accelerating gradient to obtain maximum energy gain for the beam. To achieve this, the peak electric and magnetic fields arising out of the applied RF must be minimized in the particular geometry [9]. For niobium to remain in the Meissner superconducting state, the peak magnetic field must remain below its lower critical magnetic field H_{C1}, which is $\sim$1400 G at 4.2 K. The peak magnetic field in the resonator must therefore remain below this value. Similarly, the peak electric field must be minimized to reduce loading through electron field emission. Experience has shown that peak electric fields of 30–35 MV/m are easily achievable with good clean niobium surfaces [9].

Apart from the peak electric and magnetic fields, the key parameters which need to be studied and optimized in a resonator design are: frequency, energy gain, transit time factor, stored energy, geometry factor, shunt impedance and electron multipacting. All these parameters cannot be optimized individually, independent of each other. Many of them are coupled together and therefore they have to be globally optimized. While the energy gain, geometry factor and shunt impedance must be maximized, the peak electric and magnetic fields must be minimized, maintaining a low enough value for the stored energy.

In addition to the electromagnetic parameters, the design of the resonator must aim to increase the frequency of the lowest mechanical eigenmode as high and as far away from 50 Hz as possible, to reduce microphonic-induced RF frequency jitter. The design must also ensure that liquid helium-induced pressure fluctuations do not deform the resonator substantially, which may result in large changes in its resonance frequency. Finally, the design must be such that it can be fabricated using the available infrastructure. Fabrication of superconducting niobium resonators requires some special facilities. IUAC has set up such facilities and over the past few years several niobium resonators have been successfully built and tested using this infrastructure [10].

In the following we present details of the design of the low beta quarter-wave resonator. For the electromagnetic simulation we have used the computer code CST-Microwave Studio (MWS) [11], which is a 3D electromagnetic simulator based on the finite integration technique.

2.2 *Synchronous velocity* β_0

The expected energy out of the DTL section of the HCI system is around 1.5 MeV/u, which corresponds to $\beta \approx 0.057$. As can be seen from figure 3, the energy gain on the lower velocity side of the synchronous velocity falls off rapidly when compared to the energy gain on the higher velocity side. The synchronous velocity of the low beta resonator is chosen to be 0.050 so that the lower velocity cut-off (β_{low}) will be less than 0.04 ($\sim$0.75 MeV/u), thus providing a large velocity acceptance range and sufficient cushion for tuning the beam from DTL into the superconducting Linac. Details of the energy gain and transit time factor calculations are given in the subsequent sections.

2.3 *RF Frequency*

For the effective acceleration length (L_{eff}) of the resonator to be long, the RF frequency should be as low as possible. However, this also increases the resonator height, making it mechanically unstable and also difficult to accommodate in the given height of the beam hall. Taking into account the constraint posed by the ceiling height in the beam hall, we have decided 97 MHz ($(\lambda/4) \approx 75$ cm) as the frequency for the low beta resonator also. This choice of frequency has the additional advantage that the existing clock distribution system for the entire accelerator system remains the same. In addition, the development of the electronics controls for the low beta resonator would be simpler since it will benefit from the experience gathered from operating the main Linac.

2.4 *Transit time factor calculations*

From figure 2 it is easy to see that

$$d = \frac{\beta\lambda}{2} = L_{\text{DT}} + g,$$

$$L_{\text{eff}} = L_{\text{DT}} + 2g = d + g,$$

where L_{DT} is the length of the drift tube and g is the gap length between the drift tube and the two outer tubes (ports on the housing).

The transit time factor calculations for the low beta resonator design have been done for several sets of L_{DT}, g and L_{eff} with $d\,(= \beta_0\lambda/2) = 7.73$ cm ($\beta_0 = 0.050$ and $f =$ 97 MHz). Here we only discuss the two extreme cases, namely the smallest and the largest drift tube lengths that are possible, as other combinations lie in between. Table 1 shows the values of the various parameters for these two cases.

Table 1. Drift tube length L_{DT}, gap length g and the effective acceleration length L_{eff} for the two cases.

Case No.	L_{DT} (cm)	g (cm)	L_{eff} (cm)	f (MHz)
Case I	2.5	5.23	12.96	97
Case II	5.5	2.23	9.96	97

In figure 4, the energy gain (per charge state) as a function of β for the two cases is shown. It is about 12% more in Case II compared to Case I. However, the smaller gap (g) in Case II results in a peak electric field value that is 36% more compared to Case I. If the drift tube length is reduced to 4.5 cm ($g = 3.23$ cm and $L_{eff} = 10.96$ cm), the energy gain remains about the same but the peak electric field in the gap reduces substantially and becomes only 16% more than Case I. If the drift tube length is reduced further, the energy gain begins to suffer. An optimum drift tube of length $L_{DT} = 4.5$ cm has been selected for the low beta resonator. The energy gain for this set is also shown in figure 4.

2.5 *Optimization of peak magnetic field, shunt impedance and geometry factor*

One way to minimize the peak magnetic field in a quarter-wave resonator is to taper the central coaxial line [12]. In figure 5, a schematic diagram of the linearly tapered coaxial line quarter-wave resonator is shown. Besides reducing the peak magnetic field, tapering also improves the mechanical stability of the resonator by providing a large anchoring area at the shorted end (see figure 5). However, tapering reduces the inductance thereby increases the resonance frequency, which means that the length of the coaxial line needs

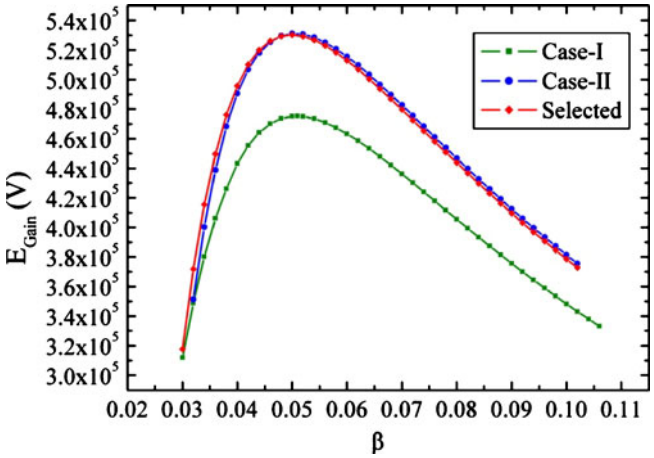

Figure 4. Energy gain per charge state vs. beta for the two cases shown in table 1. For comparison the final set selected for the design is also shown. The calculations are shown for 1 J of stored energy in the resonator.

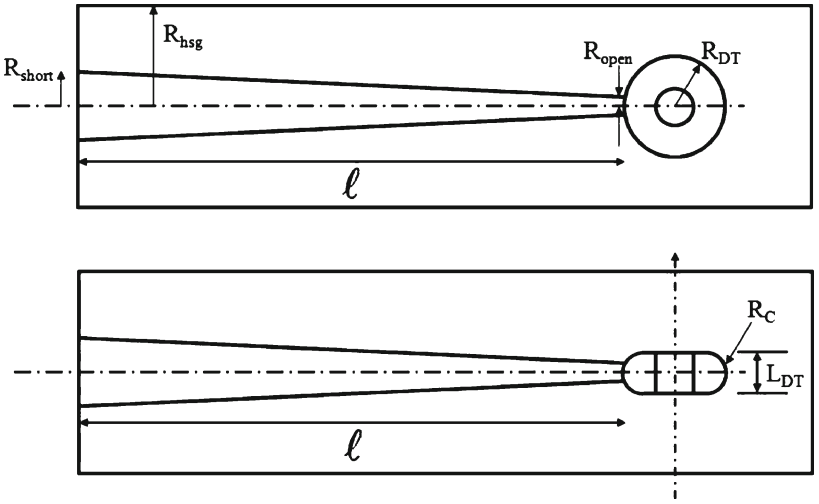

Figure 5. Schematic diagram of a linearly tapered coaxial line quarter-wave resonator. The upper and lower diagrams show the view in two perpendicular planes. The drift tube is attached at the end of the central tapered coaxial line. The dashed line with arrow through the drift tube in the lower figure indicates the beam axis, which is perpendicular to the plane of the paper in the upper figure.

to be increased to maintain the frequency. The central conductor length L_{CC}, of such a tapered line is given by

$$L_{\mathrm{CC}} = \ell + 2R_{\mathrm{DT}}.$$

The capacitance at the end of the coaxial line is decided by the size of the drift tube. By increasing it, the capacitance can be increased and the coaxial line can be foreshortened. Although this can improve the mechanical stability of the resonator, it is achieved at the cost of increasing the total stored energy (U) in it. Since the power required to phase-stabilize a resonator is equal to the product of the frequency jitter and the total electromagnetic stored energy ($P = \Delta\omega \cdot U$, $U \propto E_{\mathrm{a}}^2$), increasing the stored energy increases the power required to phase control the resonator, which can limit the on-line operating gradient of the resonator. Drift tubes of two different sizes were used for the electromagnetic modelling of the resonator on CST-Microwave Studio: drift tube radii $R_{\mathrm{DT}} = 3.25$ and 4.50 cm having the same length $L_{\mathrm{DT}} = 4.50$ cm (see figure 5). R_{open}, the radius of the coaxial line at the drift tube end (open-end) was fixed at 1.25 cm and R_{short}, the radius at the shorted-end, was increased in steps.

In figure 6, the MWS model indicating the transverse electric field along the coaxial line in the resonator, is shown. In figure 7, the peak magnetic field B_{peak} at an accelerating gradient of 1 MV/m, for different values of $R_{\mathrm{short}}/R_{\mathrm{open}}$ for the two drift tube diameters, is shown. In figures 8a and 8b, the length of the coaxial line and the shunt impedance of the resonator, as a function of the ratio of the radii, for the two different drift tube are shown.

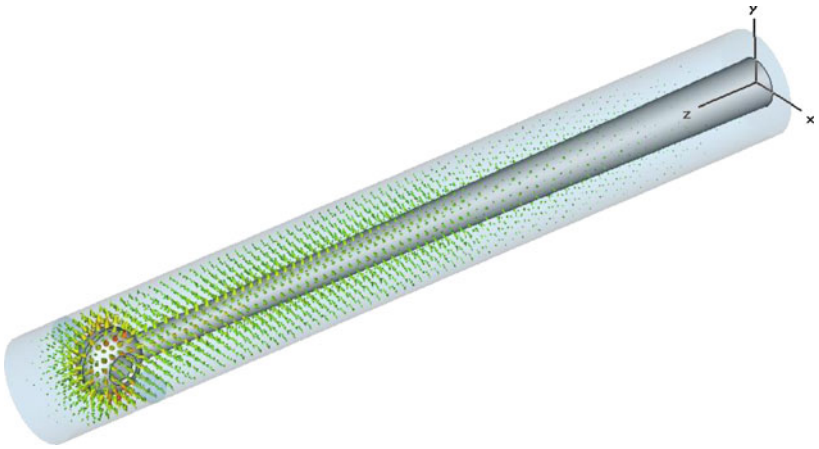

Figure 6. Results of calculations using Microwave Studio model showing the transverse electric field along the coaxial line, for the drift tube of radius $R_{\mathrm{DT}} = 3.25$ cm.

In table 2, the parameters for the two drift tube options are shown for the ratio $\left(R_{\mathrm{short}}/R_{\mathrm{open}}\right) = 2$. It can be seen that the first option with $R_{\mathrm{DT}} = 4.50$ cm is preferable since the central coaxial line is substantially shorter while the peak magnetic field and stored energy are not significantly different. Although the energy gain is higher in the second option, as we shall see in the following, the parameters improve substantially when the outer housing diameter is increased.

In the second step of the optimization, the outer housing diameter (radius R_{hsg} in figure 5) was increased in steps while maintaining the effective acceleration length $L_{\mathrm{eff}} = 10.96$ cm, to further reduce the peak magnetic field. In figure 9, MWS output of the x and

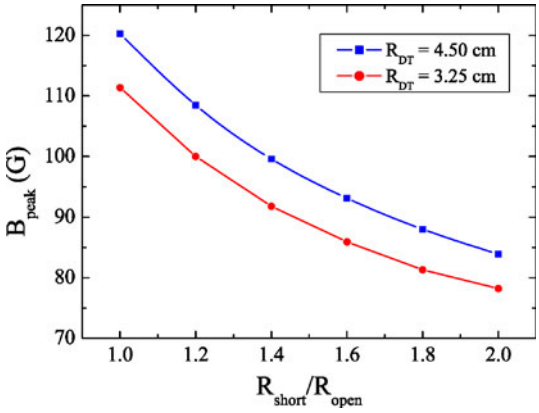

Figure 7. Peak magnetic field as a function of the ratio of the radii at the two ends of the coaxial line, for the two different drift tubes.

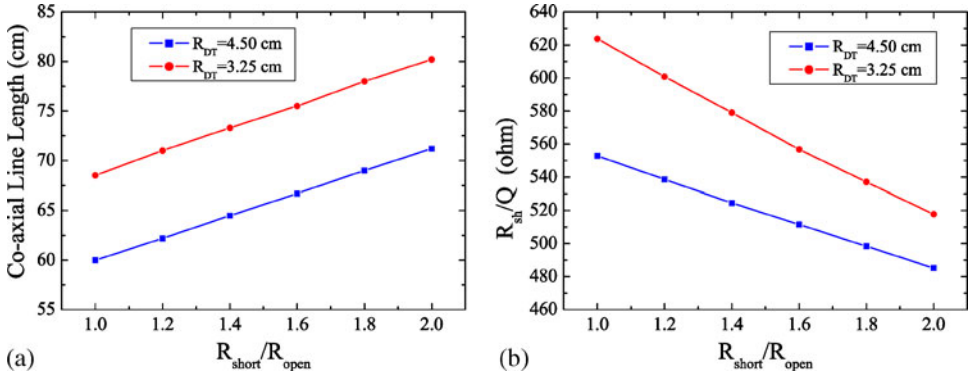

Figure 8. (**a**) Length of the coaxial line L_{CC} and (**b**) geometric shunt impedance R_{sh}/Q, as a function of the ratio of the radii at the end of the coaxial line, for the two different drift tubes.

Table 2. Parameters of the resonator for the two different drift tube options with $\left(R_{short}/R_{open}\right) = 2$. The peak magnetic field B_{peak} and stored energy U_0 are shown at an accelerating gradient of 1 MV/m. The energy gain is shown for a stored energy of 1 J in the resonator.

Parameter	$R_{DT} = 4.50$ cm	$R_{DT} = 3.25$ cm
B_{peak}	84 G	78 G
L_{CC}	71.5 cm	80 cm
R_{sh}/Q	485 Ω	518 Ω
QR_s	11 Ω	11 Ω
E_{Gain}	0.545 MV	0.561 MV
U_0	36.7 mJ	33.4 mJ

y-components of the magnetic field along the tapered coaxial line for $R_{DT} = 4.5$ cm is shown. In figures 10a and 10b, the peak magnetic field and shunt impedance respectively are shown as functions of the outer housing diameter for $(R_{short}/R_{open}) = 2$, for both the drift tubes sizes. In figures 11a and 11b, the central coaxial line length and geometry factor QR_s respectively are shown as functions of the outer housing diameter for $\left(R_{short}/R_{open}\right) = 2$, for both the drift tubes sizes. The calculations have been performed up to the outer housing diameter of 16 cm, since beyond this value the real estate gradient, which is the average accelerating gradient over the entire length of the real accelerator, begins to suffer.

In table 3, the parameters for both the options, $R_{DT} = 4.50$ and 3.25 cm are shown. As can be seen, the values of peak magnetic field, stored energy and geometry factor are quite close in both the options. Although the energy gain is slightly more (∼2.5%) in the second option, the coaxial line is longer by about 8%. As mentioned earlier, the ceiling

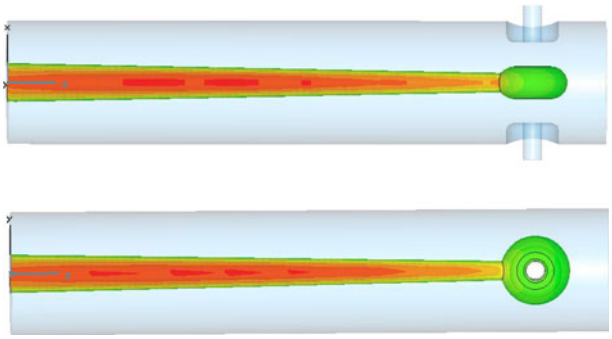

Figure 9. MWS output of the x- and y-components of the magnetic field along the tapered coaxial line, for the drift tube of radius $R_{\mathrm{DT}} = 4.50$ cm.

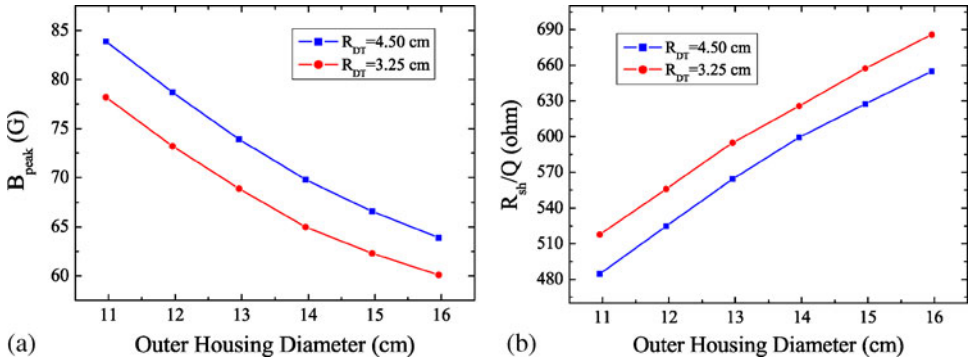

Figure 10. (**a**) Peak magnetic field and (**b**) geometric shunt impedance, as a function of outer housing diameter for $\left(R_{\mathrm{short}}/R_{\mathrm{open}}\right) = 2$, for the two different drift tubes.

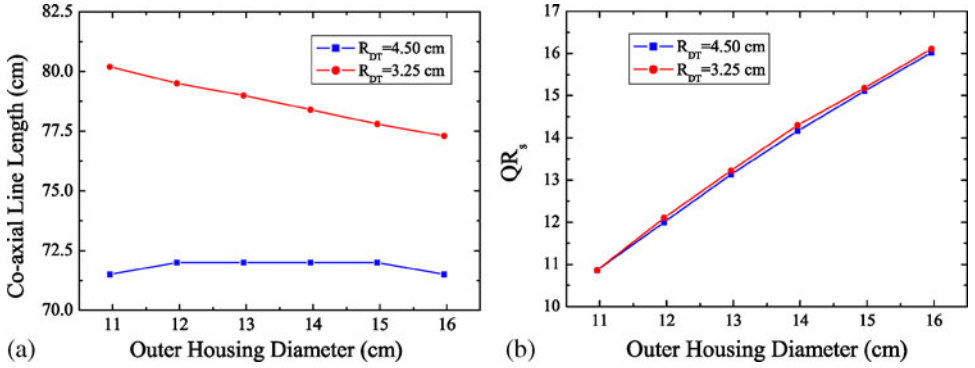

Figure 11. (**a**) Coaxial line length L_{CC} and (**b**) geometry factor $\mathrm{QR_s}$, as a function of the outer housing diameter for $\left(R_{\mathrm{short}}/R_{\mathrm{open}}\right) = 2$, for the two different drift tubes.

Table 3. Parameters of the resonator for the two different drift tube options with $\left(R_{\text{short}}/R_{\text{open}}\right) = 2$ and outer housing diameter = 16 cm. The peak magnetic field B_{peak} and stored energy U_0 are shown at an accelerating gradient of 1 MV/m. The energy gain is shown for a stored energy of 1 J in the resonator.

Parameter	R_{DT}= 4.50 cm	R_{DT}= 3.25 cm
B_{peak}	64 G	60 G
L_{CC}	71.5 cm	77.3 cm
OH Diameter	16 cm	16 cm
R_{sh}/Q	655 Ω	686 Ω
QR_{s}	16 Ω	16.1 Ω
E_{Gain}	0.631 MV	0.646 MV
U_0	28.8 mJ	26.6 mJ

height in the beam hall where the low beta module will be located, constrains the overall height of the resonator. Hence the first option, with $R_{\text{DT}} = 4.50$ cm was finally chosen for the low beta resonator design.

2.6 *Optimization of peak electric field*

The peak electric field occurs on the drift tube of the central coaxial line and its value is decided by the corner radius R_{C} on the drift tube (see figure 5). Since $L_{\text{DT}} = 4.50$ cm, the maximum corner radius that can be provided on the drift tube is 2.25 cm. In figure 12, the peak surface electric field at an accelerating gradient of 1 MV/m as a function of the

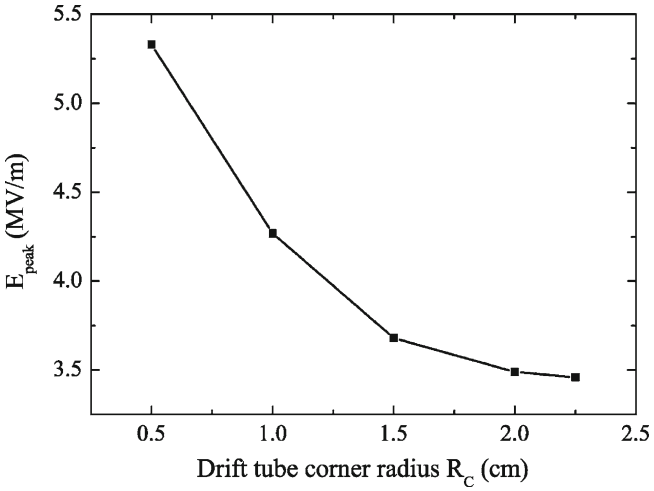

Figure 12. Peak surface electric field at 1 MV/m accelerating gradient as a function of drift tube corner radius R_{C}.

corner radius R_C, is shown. As can be seen, the values of the peak electric field are not substantially different for $R_C = 2.0$ and 2.25 cm. Since the drift tube will be die-formed in two halves and electron beam welded, it has been decided to keep $R_C = 2.0$ cm, which will provide a proper circumferential welding joint for the two halves.

2.7 *Multipacting*

Electron multipacting in RF resonators makes it difficult to power them and the design should try to minimize the probability of its occurrence. Two-point multipacting in TEM class structures occurs if the combination of gap length g (see figure 2) in the high electric field region and the RF frequency of the resonator is such that the electrons gain energy in the range 100–1000 eV where the secondary electron emission coefficient for niobium is more than 1. The electron energy is given by [9]

$$K_n = \frac{2e^2 V_n}{m_e \omega^2 g^2},$$

where $V_n = \left(g^2\omega^2 m_e/(2n-1)\pi e\right)$ is the gap voltage at which two-point multipacting of order n can occur, e and m_e are the charge and mass of the electron respectively and $\omega = 2\pi f$. For $n = 1$, the energy in electron-volts is given by $K_n = 4.55 \times 10^{-3} f^2 g^2$ eV, where f is in MHz and g is in cm.

Apart from the proper selection of g and f, it is also important to avoid cylindrical symmetry in the high electric field region and minimize the total surface area over which electron multipacting can occur. Tapering of the central coaxial line and geometry of the drift tube in the present design of the low beta resonator have been made keeping this in consideration.

2.8 *Final optimization of the resonator*

In changing the geometry for the optimization of all the relevant parameters, we find that the synchronous velocity slightly shifts from the starting value. In order to bring it back to the design value ($\beta = 0.050$), some minor adjustments in the drift tube length and gap (L_{DT} and g) have to be made. This, however, does not change other parameters significantly. Although reducing L_{DT} or g reduces the synchronous velocity, detailed analysis shows that the change in g (and therefore L_{eff}) brings about a faster change in the synchronous velocity compared to change in L_{DT}. For the final design of the low beta resonator, however, both L_{DT} and g have been slightly changed for adjusting the synchronous velocity β_0. In table 4, the parameters of the final design are shown. In figure 13, the transit time factor $T(\beta)$ as a function of β for the final design of the resonator, is shown. It is almost flat over the range $\beta = 0.049$–0.052. The $\Delta\beta$ value is nearly 0.072, suggesting that the low beta resonator design has a broad velocity acceptance. The accelerating electric field profile along the beam axis is shown in §3, which describes the room-temperature copper model of the resonator.

Table 4. Final parameters of the low beta resonator design. The stored energy U_0, peak magnetic and electric fields B_{peak} and E_{peak} respectively are shown at 1 MV/m accelerating gradient. E_a and V_{Gain} are shown at 1 J of stored energy in the resonator.

Parameter	Value
β_0	0.051
f	97 MHz
L_{eff}	10.4 cm
L_{DT}	4.2 cm
OH Diameter	15.9 cm
L_{CC}	72 cm
U_0	26 mJ
B_{peak}	64.2 G
E_{peak}	3.4 MV/m
R_{sh}/Q	650
QR_s	16.1
E_a at 1 J	6.2 MV/m
V_{Gain} at 1 J	0.63 MV

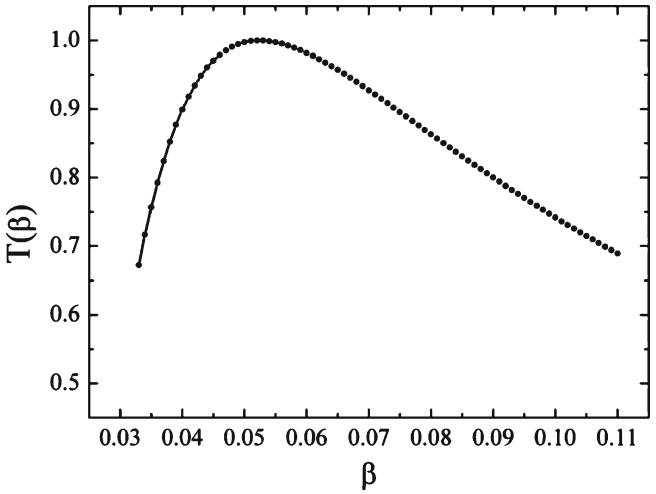

Figure 13. Transit time factor as a function of β for the final design of the low beta resonator.

2.9 *Frequency sensitivity*

The two major sub-assemblies of the low beta resonator which determine its resonance frequency, namely the outer housing and central coaxial line, can only be fabricated within certain dimensional tolerances. In order to understand the tolerance limits on them, the

frequency sensitivity of the sub-assemblies was studied. This information is also useful in selecting niobium of proper thickness to reduce the deformation produced in them from liquid helium-induced pressure fluctuations, which translate into RF frequency jitter. In addition, the frequency sensitivity is also useful in understanding the expected change in the RF frequency of the resonator after electropolishing it.

For the outer housing, the frequency sensitivity is calculated to be about -55 kHz/mm, whereas for the central coaxial line it is $+410$ kHz/mm.

2.10 *Tunability*

For online operation in the Linac, all the resonators must be tuned to the same frequency. The quarter-wave resonators in the superconducting Linac use niobium slow tuner bellows for tuning the resonators online [2]. The slow tuner is mounted at the drift tube end of the resonator and is moved in and out by pressurizing with helium gas or evacuating the bellows. This changes the capacitance at the drift tube end of the resonator and changes its resonance frequency. For a 20 psi change in pressure, a total displacement of 3 mm of the bellows is achieved. Extensive work has been done over the last several years to make the slow tuners reliable and the work has produced very good results. In addition, the electronics control system of the slow tuner has also undergone major improvements.

In view of this, we propose to use the same design for slow tuner bellows for the low beta resonators also. The frequency tunability of the low beta resonator has been simulated using Microwave Studio. For a 3 mm displacement in the bellows the estimated frequency change is around 100 kHz, which is sufficient to tune the resonators online.

2.11 *Mechanical and engineering design*

The mechanical design of the coaxial line resonator aimed at increasing the frequency of the lowest eigenmode as high and as far away from 50 Hz as possible to reduce microphonic-induced RF frequency jitter. Finite element analysis was done using the computer code ANSYS multiphysics [13] and the coaxial line was modelled to study the vibration modes and their frequencies. In addition, deformations in the mechanical structure of the resonator arising from liquid helium-induced pressure fluctuations, which translate into RF frequency jitter, were also studied.

The tapered coaxial line in the resonator would be fabricated with 3 mm thick niobium to make the structure sufficiently stiff. Its mechanical frequency can be increased by reducing the mass at the drift tube end, and hence a thickness of 1.5 mm was chosen for the drift tube. For increasing the mechanical frequency further, the wall thickness of the coaxial line at the open end would be reduced from 3 mm to 1.5 mm by machining out the material from its inside. In figure 14, the frequency of the lowest eigenmode as a function of the length of the central coaxial line over which the wall thickness is reduced, is shown. As can be seen, the frequency increases from 61 Hz to 64.6 Hz when the wall thickness is reduced over 120 mm. This value is sufficiently far away from 50 Hz, and should reduce the microphonic-induced RF frequency jitter in the resonator.

In the closed loop refrigeration for the superconducting Linac, the liquid helium system is maintained above 1 bar pressure. During online operation of the Linac, the pressure

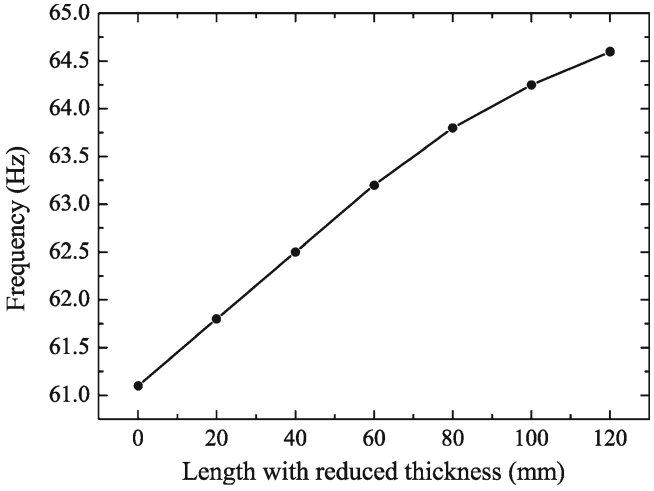

Figure 14. Frequency of the lowest mechanical eigenmode as a function of the length over which the wall thickness of the central coaxial line is reduced from 3 to 1.5 mm.

fluctuations in this system have been measured to be about 25 mbar [14]. It is reasonable to expect a similar value in the low beta module also. The deformation in niobium housings of 2, 3 and 4 mm wall thickness due to pressure fluctuations of 50 mbar (twice the measured value) were calculated using finite element analysis. Using the frequency sensitivity value, discussed earlier, this translates to 4, 3 and 2 Hz RF frequency fluctuation respectively. Similarly for the top flange, calculations done with 10, 12.7 and 15 mm thick niobium indicated that the RF frequency would fluctuate by 13, $5\frac{1}{2}$ and 4 Hz respectively for a pressure fluctuation of 50 mbar. Increasing the thickness of niobium reduces the heat transport across it and increases the cost of the material. Considering all these arguments, we have chosen 3 mm thick material for the outer housing and 12.7 mm ($\frac{1}{2}''$) thick material for the top flange. The total fluctuation due to the simultaneous deformation in the outer housing and top flange would be less than the bandwidth of the loaded resonator, which is typically set around 20 Hz.

The niobium resonator would be closely jacketed with an outer stainless steel vessel which will contain liquid helium needed for cooling the resonator. This design, originally developed for the QWRs used in the IUAC superconducting Linac [5], has been adopted by many groups on several different resonator designs around the world. For joining niobium to stainless steel (SS), flanges made of explosively bonded Nb–SS composite material will be used. The resonator would be anchored at the open-end (the drift tube end) and free to move at the top. To take care of the differential contraction between niobium and stainless steel when the resonator is cooled down from room temperature to 4.2 K, the composite material flanges would be used along with stainless steel bellows. This design, developed originally for the IUAC-QWR and modified subsequently [15], is very reliable. In figure 15, a cut-away view of the low beta resonator design along with its outer stainless steel vessel, is shown.

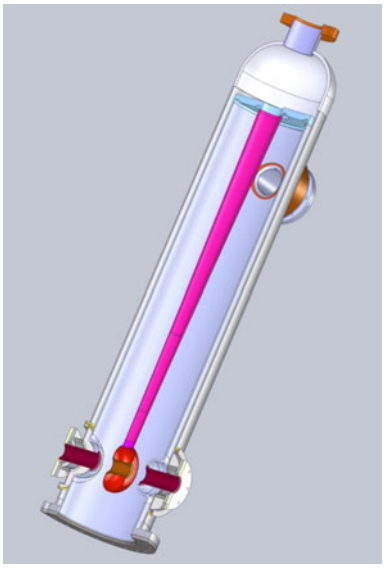

Figure 15. Cut away 3D view of the low beta resonator design showing niobium components inside and the stainless steel vessel outside.

2.12 *Number of resonators needed*

The number of resonators needed in the low beta module for reaching the required velocity for injection into the superconducting Linac, is given by

$$n_{\text{res}} = \frac{466.5\left(\beta_{\text{f}}^2 - \beta_{\text{i}}^2\right)(A/q)}{E_{\text{a}} L_{\text{eff}} T(\beta) \sin\phi},$$

where β_{i} is the injection velocity, β_{f} is the final velocity and ϕ is the phase angle of the RF with respect to the beam bunch. E_{a} and L_{eff} are in MV/m and metre respectively. The phase angle is usually set so that the beam is accelerated without blowing up the longitudinal emittance. Assuming an accelerating gradient of 5 MV/m, phase angle of 80° (i.e. phase offset of 10°) and an average value of $T(\beta) = 0.97$ over the velocity range, the number of resonators required to accelerate from $\beta_{\text{i}} = 0.040$ to $\beta_{\text{f}} = 0.055$ is about eight. Given the performance of the resonators built at IUAC [16], this gradient is realistically achievable. The existing cryomodules in the superconducting Linac house eight resonators each. Since the outer diameters of the low beta resonator and the quarter-wave resonators used in the superconducting Linac are the same, a cryomodule similar to the existing design can be developed for the low beta module also.

3. Copper model

A copper model has been built for validating the electromagnetic parameters of the low beta resonator design before starting work with niobium. The copper model of the

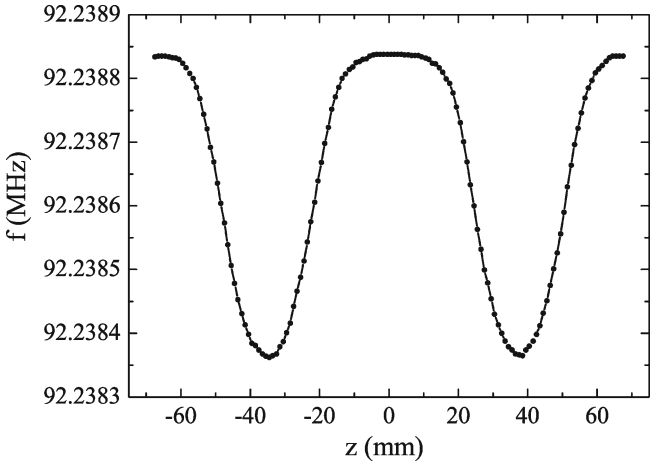

Figure 16. Frequency as a function of the bead position when a spherical dielectric bead is pulled through the beam axis of the resonator.

resonator exactly mimicked the design except that the drift tube was rolled into a cylinder without the corner radius R_C (see figure 5), which is primarily provided to reduce the peak surface electric field. This minor change was made to avoid making a forming die to fabricate a drift tube of the exact geometry. It, however, meant that the expected frequency would be lower than the design frequency due to the increase in the drift tube capacitance. The modified resonator geometry was also modelled on Microwave Studio to calculate the resonance frequency, which came out to be 92.54 MHz. However, the other parameters of the resonator did not change significantly.

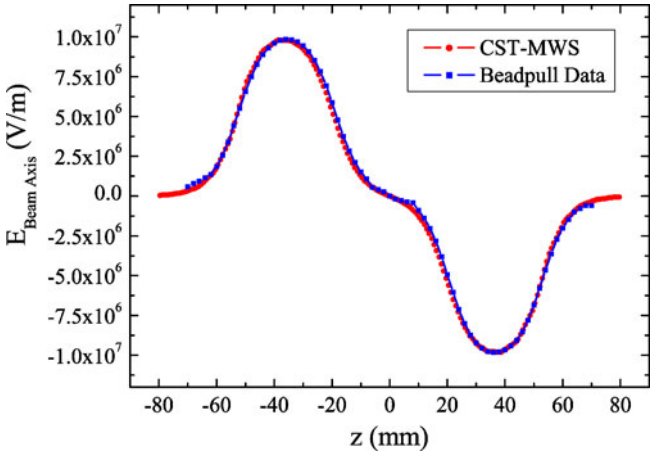

Figure 17. Electric field profile along the beam axis of the copper model of the resonator. For comparison, data from Microwave Studio calculations are also shown.

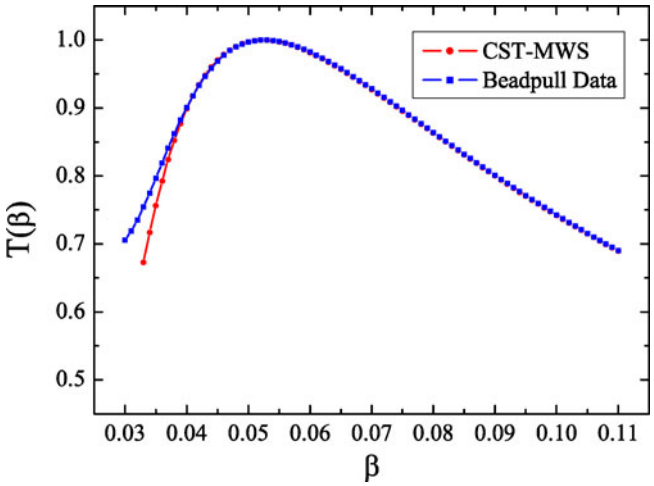

Figure 18. Comparison of transit time factor as a function of β calculated from the bead pull data with the results from MWS calculations.

3.1 *Bead pull measurements*

Bead pull measurements [17] were performed on the copper model to measure the change in the resonator frequency as a function of the bead position. From this data the on-axis electric field profile, stored energy, energy gain, transit time factor and shunt impedance were calculated. In figure 16, the RF frequency as a function of the position of the bead is shown, when a spherical dielectric bead is pulled through the beam axis of the resonator. In figure 17, the electric field profile along the beam axis, calculated from the frequency perturbation data, is shown. For comparison, the field generated by Microwave Studio is also shown in the figure. In figure 18, the transit time factor calculated from the electric field profile is shown along with the values calculated using Microwave Studio code.

Table 5. Calculated and measured values of the parameters from the bead pull measurement. The higher value of stored energy in the copper model is due to the slightly larger capacitance of the drift tube.

	Calculated	Measured
f	92.54 MHz	92.25 MHz
β_0	0.051	0.051
U_0	28.7 mJ	27 mJ
R_{sh}/Q	650	658
Δf_{ST}	100 kHz	110 kHz

In addition, the frequency tunability of the resonator was also measured using a mock slow tuner and displacing it by 3 mm to mimic the motion of the bellows. In table 5 the various parameters measured on the copper model are shown. The agreement between the calculated and measured values is excellent, thus validating the electromagnetic design of the resonator.

4. Conclusions

A TEM class resonator optimized for $\beta = 0.050$ operating at 97 MHz, has been designed for the high current injector at IUAC. This resonator has the highest frequency among all the superconducting accelerating structures designed to operate at such a low velocity for heavy ions. The electromagnetic design has been done to arrive at an optimal design and a copper model has been built and tested to validate it. Mechanical analysis of the structure has been done to identify the vibrational modes and the engineering design has been completed. Fabrication of two niobium prototype resonators has been started. Most of the dies and tooling required for fabricating the components have been made and some niobium components for the prototype resonators have been fabricated. We expect to perform the first cold test of the resonator in the next few months.

Acknowledgements

The authors would like to thank Mr K K Mistri for his help in fabricating the copper model of the resonator and Mr Rajeev Mehta for helping with the bead pull set-up and measurements. The authors thank Mr Jimson Sacharias for his help in creating the engineering model and for making the fabrication drawings.

References

[1] D Kanjilal *et al*, *Nucl. Instrum. Methods* **A328**, 97 (1993)
[2] S Ghosh *et al*, *Phys. Rev. Special Topics – Accelerators & Beams* **12**, 040101 (2009)
[3] R Geller, *Electron cyclotron resonance ion sources and ECR plasmas* (Institute for Physics Publishing, Bristol, 1996)
[4] Amit Roy, *Pramana – J. Phys.* **57(2 & 3)**, 659 (2001)
[5] K W Shepard, A Roy and P N Potukuchi, *Proceedings of the 1997 Particle Accelerator Conference* (Vancouver, B.C., Canada, 1997) p. 3072
[6] L M Bollinger, *Proceedings of the XIX International Linac Conference (LINAC98)* (Chicago, USA, 1998) p. 3
[7] M P Kelly, *Proceedings of the 2006 Linear Accelerator Conference (LINAC06)* (Knoxville, TN, USA, 2006) p. 23
[8] A Facco, TESLA Technology Collaboration Meeting, April 2010, Fermi National Accelerator Laboratory, USA, website: http://conferences.fnal.gov/ttc10/
[9] Hasan Padamsee, Jens Knobloch and Tom Hays, *RF superconductivity for accelerator* (Wiley-VCH Verlag GmbH & Co., KGaA, Weinheim, 2008) 2nd edn
[10] Prakash N Potukuchi, *Proceedings of the 14th International Conference on RF Superconductivity (SRF2009)* (Berlin, Germany, 2009) p. 502
[11] Computer Simulation Technology, Darmstadt, Germany, website: www.cst.com

[12] I Ben-Zvi and J M Brennan, *Nucl. Instrum. Methods* **212**, 73 (1983)
[13] ANSYS, Inc., Canonsburg, PA, USA, website: www.ansys.com
[14] S Kar, Cryogenics Group-IUAC, Private Communication
[15] P N Prakash *et al*, *Proceedings of the Asian Particle Accelerator Conference (APAC2004)* (Gyeongju, Korea, 2004) p. 684
[16] Prakash N Potukuchi, *Proceedings of the 5th DAE-BRNS Indian Particle Accelerator Conference (InPAC2011)* (IUAC, New Delhi, 2011) website: www.iuac.res.in/InPAC2011/
[17] L C Maier and J C Slater, *J. Appl. Phys.* **23(1)**, January 1952